NASA/TM—2018–220181

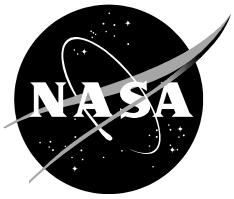

TESS Data Release Notes:
Sector 3, DR4

Michael M. Fausnaugh
Kavli Institute for Astrophysics and Space Science, Massachusetts Institute of Technology, Cambridge, Massachusetts

Douglas A. Caldwell
SETI Institute, Mountain View, California

Jon M. Jenkins
Ames Research Center, Moffett Field, California

Jeffrey C. Smith, Joseph D. Twicken
SETI Institute, Mountain View, California

Roland Vanderspek
Kavli Institute for Astrophysics and Space Science, Massachusetts Institute of Technology, Cambridge, Massachusetts

John P. Doty
Noqsi Aerospace Ltd, Billerica, Massachusetts

Jie Li
SETI Institute, Mountain View, California

Eric B. Ting
Ames Research Center, Moffett Field, California

Joel S. Villasenor
Kavli Institute for Astrophysics and Space Science, Massachusetts Institute of Technology, Cambridge, Massachusetts

February 4, 2019

Acknowledgements

These Data Release Notes provide information on the processing and export of data from the Transiting Exoplanet Survey Satellite (TESS). The data products included in this data release are target pixel files, light curve files, collateral pixel files, full frame images (FFIs), cotrending basis vectors (CBVs), and Data Validation (DV) reports, time series, and associated xml files.

These data products were generated by the TESS Science Processing Operations Center (SPOC, Jenkins et al., 2016) at NASA Ames Research Center from data collected by the TESS instrument, which is managed by the TESS Payload Operations Center (POC) at Massachusetts Institute of Technology (MIT). The format and content of these data products are documented in the Science Data Product Description Document (SDPDD)[1]. The SPOC science algorithms are based heavily on those of the Kepler Mission science pipeline, and are described in the Kepler Data Processing Handbook (Jenkins, 2017).[2] The Data Validation algorithms are documented in Twicken et al. (2018) and Li et al. (2019). The TESS Instrument Handbook (Vanderspek et al., 2018) contains more information about the TESS instrument design, detector layout, data properties, and mission operations.

The TESS Mission is funded by NASA's Science Mission Directorate.

This report is available in electronic form at
https://archive.stsci.edu/tess/

[1] https://archive.stsci.edu/missions/tess/doc/EXP-TESS-ARC-ICD-TM-0014.pdf
[2] https://archive.stsci.edu/kepler/manuals/KSCI-19081-002-KDPH.pdf

1 Observations

TESS Sector 3 observations include physical orbits 13 and 14 of the spacecraft around the Earth. During this time, experiments to improve the spacecraft pointing were conducted. Although imaging and light curve data collected during these testing periods are included in this data release, the data used for science analysis excludes these time periods. Useful data was collected over 20.4 days, with a 1.12 day pause during perigee passage for data downlink. See §1.2 for more details.

Table 1: Sector 3 Observation times

	UTC	TJD[a]	Cadence #
Orbit 13 start	2018-09-20 12:56:15	1382.03987	111297
Science Data Start	2018-09-24 09:30:00	1385.89663	114078
Orbit 13 end	2018-10-03 23:30:02	1395.47997	120978
Orbit 14 start	2018-10-05 02:30:02	1396.60497	121788
Science Data End	2018-10-14 19:00:00	1406.29247	128763
Orbit 14 end	2018-10-17 21:17:58	1409.38829	130988

[a] TJD = TESS JD = JD - 2,457,000.0

The spacecraft was pointing at RA (J2000): 36.314 ; Dec (J2000): 44.259 ; Roll: 213.04 . Two-minute cadence data were collected for 16,000 targets, and full-frame images were collected every 30 minutes. See the TESS project Sector 3 observation page[3] for the coordinates of the spacecraft pointing and center field-of-view of each camera, as well as the detailed target list. Fields-of-view for each camera with all two-minute targets can be found at the TESS Guest Investigator Office observations status page[4].

1.1 Notes on Individual Targets

Three very bright stars (Tmag $\lesssim$ 2) with large pixel stamps were not processed in the photometric pipeline. Target pixel files with raw data are provided, but no light curves were produced. The affected TIC IDs are 38877693, 114434141, and 238196512.

Four targets were erroneously placed on the wrong CCD in Camera 4. A target pixel file for each target is provided, although the raw pixel data does not contain the target designated in the file names. No optimal apertures or light curves were produced. The affected TIC IDs are 260192532, 150065151, 150106553, and 141423536.

One target (300015238) had a very bright star nearby (300015239). The contaminating flux for this object is very large and the pipeline assigns it a disjoint photometric aperture, which likely causes uncorrected systematic errors in the light curve.

One target (220393543) had a small aperture selected (25x25 pixels) that did not fully capture the bleed trails.

One target (29928567, Tmag = 8.10) was selected by a GI program with a proper motion override. The RA/Dec proper motion was set to 3321.0/562.0 mas/year (the TIC lists the

[3] https://tess.mit.edu/observations/sector-3

[4] https://heasarc.gsfc.nasa.gov/docs/tess/status.html

RA/Dec proper motion as 0.0/0.0 mas/year). However, this change was not propagated to the SPOC pipeline, and the calculated optimal aperture is therefore offset from the source by several pixels. The target is correctly centered in the target pixel file, but the light curve file does not contain measurements from this source because of the aperture shift.

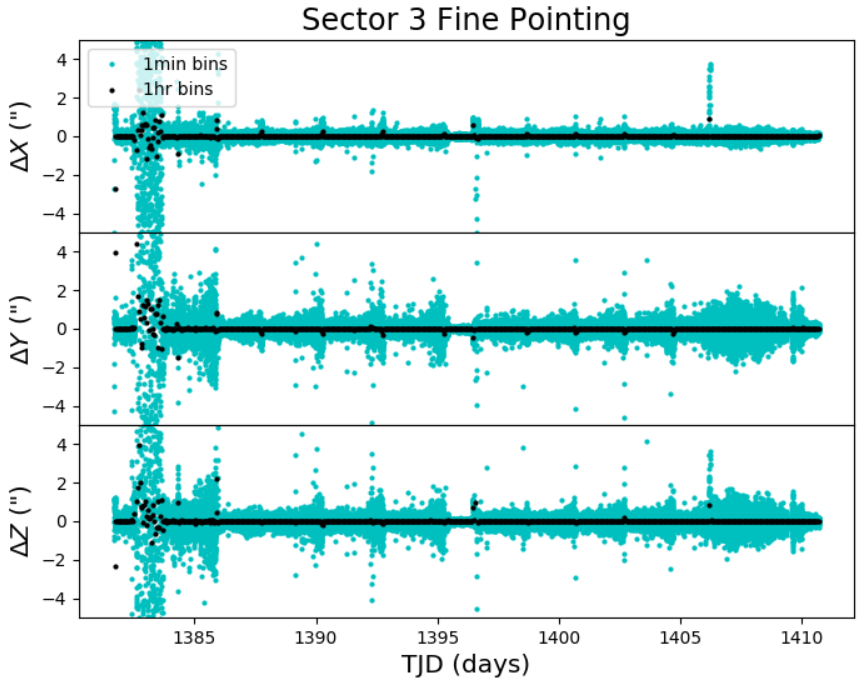

Figure 1: Guiding corrections based on spacecraft fine pointing telemetry. The delta-quaternions from each camera have been converted to spacecraft frame, binned to 1 minute and 1 hour, and averaged across cameras. Long-term trends (such as those caused by differential velocity aberration) have also been removed. The ΔX/ΔY directions represent offsets along the the detector rows/columns, while the ΔZ direction represents spacecraft roll. The large dispersion in the first 4 days and last 4 days of observations are during periods of ACS testing. For the remaining time intervals, the sudden decreases in dispersion every 2.5 days mark the momentum dumps. See §1.2 for details.

1.2 Spacecraft Pointing and Momentum dumps

In Sector 3, the TESS operations team carried out several experiments on the attitude control system (ACS) to improve pointing stability. Tests were conducted during the perigee passages after orbits 12, 13 and 14, as well as the first 3 days of orbit 13 and the last 3 days of orbit 14. During these times, the ACS feedback loop was altered and the calibration parameters tuned. The jitter profile during these times differs substantially from the normal data collection mode, which used the same ACS configuration as in Sectors 1 and 2. Imaging and light curve data during these tests is provided for completeness, but has limited use for

scientific applications. Time intervals during ACS testing were therefore flagged with bit 8 (Manual Exclude) and omitted from analysis in the SPOC pipeline.

Valid data in the standard ACS configuration were collected between TJD 1385.8966 and 1395.4800 in orbit 13 and between TJD 1396.6050 and 1406.2925 in orbit 14, spanning 20.4 days of useful observations. There is a 1.12 day gap during perigee passage for data downlink and additional ACS testing.

As in Sector 1, the reaction wheel speeds were reset to low values with momentum dumps every 2.5 days. Cadences during momentum dumps have bit 6 set (Reaction Wheel desaturation Event) and bit 8 set (Manual Exclude). These intervals include a 20 minute buffer for Fine Pointing mode to resume.

Figure 1 summarizes the pointing history over the course of the sector based on Fine Pointing telemetry. The very large dispersion in the first 4 days of the sector is due to ACS testing, as is the increase in dispersion in the last four days. The very low dispersion near the middle of the sector is also due to ACS testing during the orbit 13/14 perigee passage. Science data were collected for the remaining intervals, during which time the sudden decreases in dispersion every 2.5 days mark the momentum dumps.

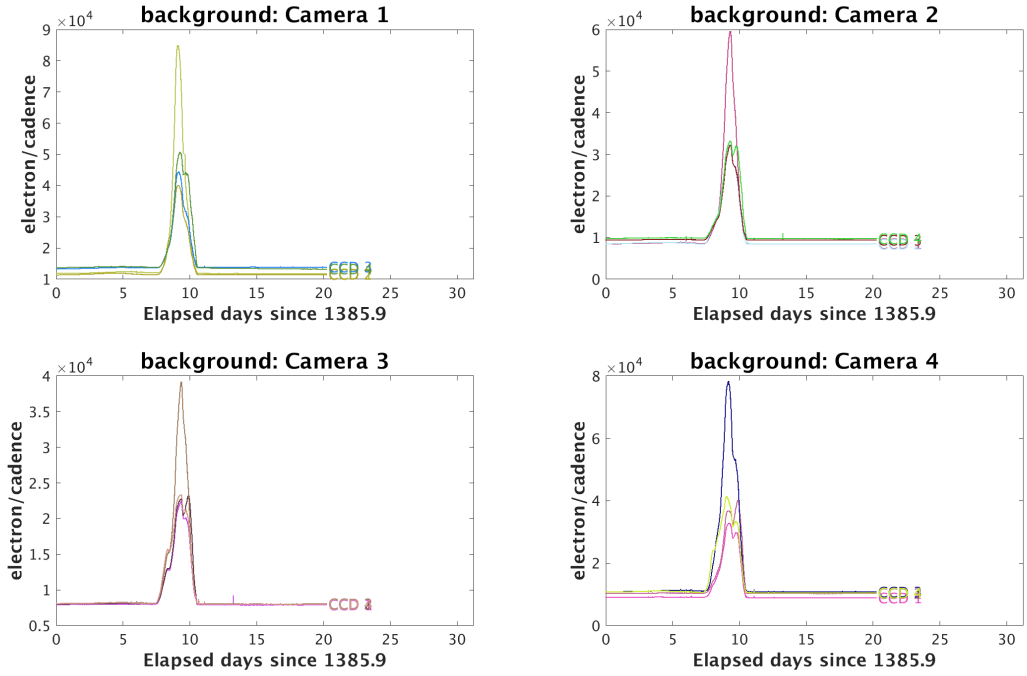

Figure 2: Median background flux across all targets on a given CCD in each camera. The changes are caused by variations in the orientation and distance of the Earth and Moon. The bump near the middle of the sector is caused by the Earth rising above the sunshade.

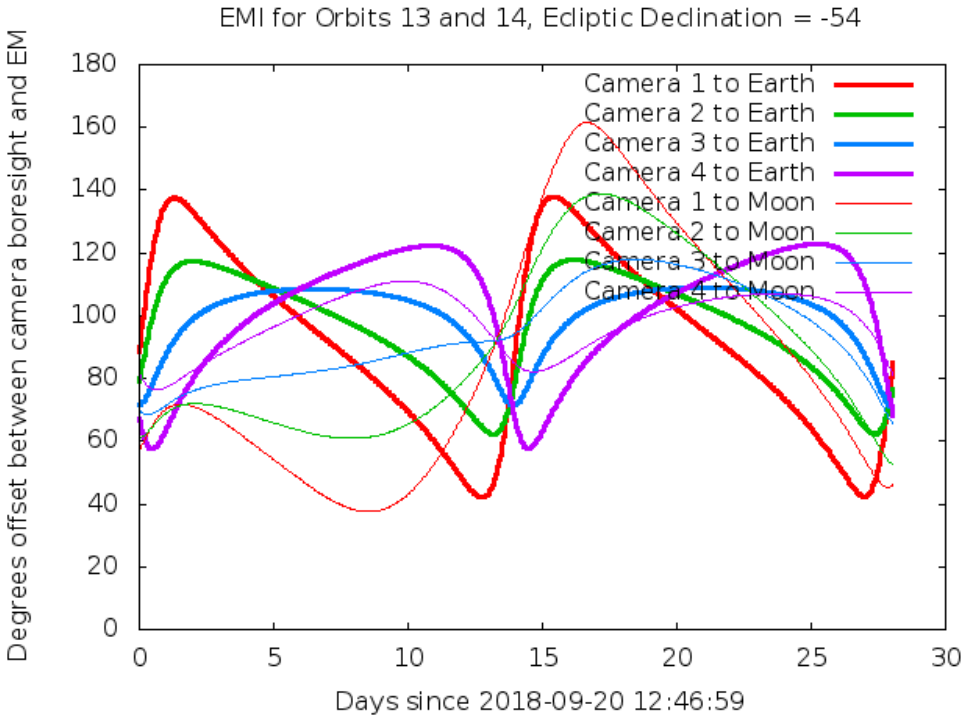

Figure 3: Angle between the four camera boresights and the Earth/Moon as a function of time. When the Earth/Moon moves within 37 of a camera's boresight, scattered light patterns and complicated features such as glints may appear. At larger angles, low level patchy features may appear. This figure can be used to identify periods affected by scattered light and the relative contributions of the Earth and Moon to the background. However, the background intensity and locations of scattered light features depend on additional factors, such as the Earth/Moon azimuth and distance from the spacecraft.

1.3 Scattered Light

Figure 2 shows the median value of the background estimate for all targets on a given CCD as a function of time. Figure 3 shows the angle between each camera's boresight and the Earth or Moon—this figure can be used to identify periods affected by scattered light and the relative contributions of the Earth and Moon to the image backgrounds. In Sector 3, the main stray light feature is caused by the Earth rising above the sunshade near the end of each orbit, resulting in an enhancement of the stray light over parts of each camera's FOV.

2 Data Anomaly Flags

See the SDPDD (*x*9) for a list of data quality flags and the associated binary values used for TESS data, and the instrument handbook for a more detailed description of each flag.

The following flags were not used in Sector 3: bits 1, 2, 7, 9, 11, and 12 (Attitude Tweak, Safe Mode, Cosmic Ray in Aperture, Discontinuity, Cosmic Ray in Collateral Pixel, and Straylight).

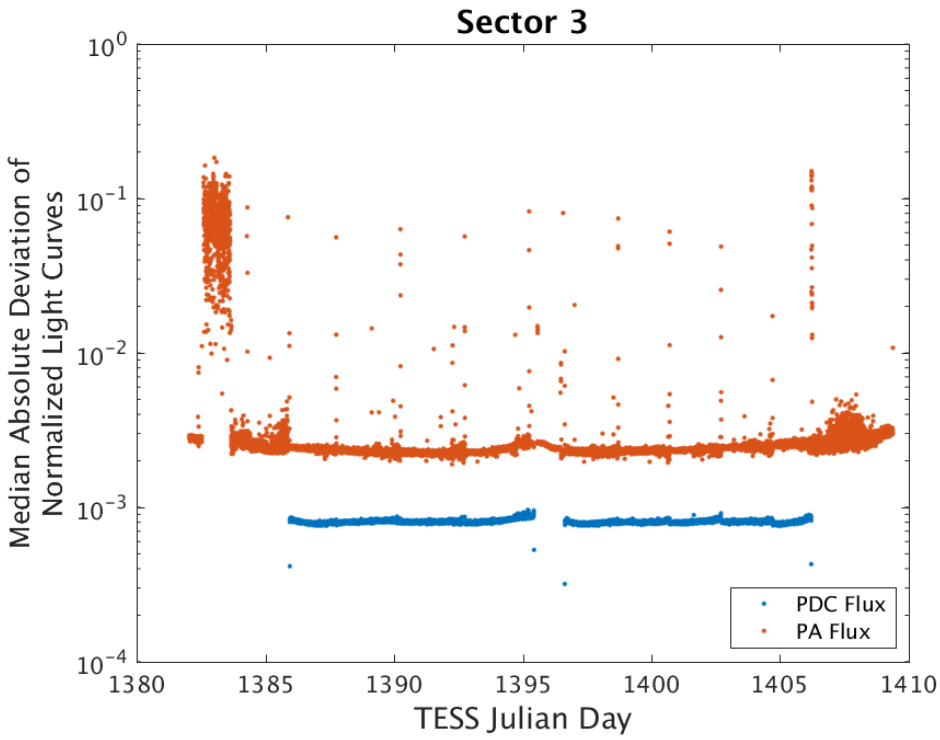

Figure 4: Median absolute deviation (MAD) for the 2-minute cadence data from Sector 3, showing the performance of the cotrending after identifying Manual Exclude data quality flags. The MAD is calculated in each cadence across stars with flux variations less than 1% for both the PA (red) and PDC (blue) light curves, where each light curve is normalized by its median flux value. The scatter in the PA light curves is much higher than that for the PDC light curves, and the outliers in the PA light curves are largely absent from the PDC light curves due to the use of the anomaly flags. Note that the MAD for some of the cadences in the PDC light cuves have values slightly above 1 10 ^{3} threshold after reprocessing. Note also that the first and last cadences in each orbit are treated as gaps by PDC.

Cadences marked with bits 3, 4, and 6 (Coarse Point, Earth Point, and Reaction Wheel Desaturation Event) were marked based on spacecraft telemetry.

Cadences marked with bit 5 and 10 (Argabrightening Events and Impulsive Outlier) were identified by SPOC pipeline results. Bit 5 marks a sudden change in the background measurements. In practice, all bit 5 flags are caused by the unstable pointing at times near momentum dumps. Bit 10 marks an outlier identified by PDC and omitted from the cotrending procedure.

Cadences marked with bit 8 (Manual Exclude) are ignored by PDC, TPS, and DV for cotrending and transit searches. In Sector 3, these cadences were identified using a similar procedure as in Sector 1. First, all cadences during periods of ACS testing and with pointing excursions >21 arcseconds (1 pixel) were flagged for manual exclude. These cadences were excluded in an initial run of the pipeline, and the resulting light curves were corrected for systematic errors using PDC. We then calculated the median absolute deviation (MAD) of the normalized light curves at each cadence for a collection of quiet stars with average

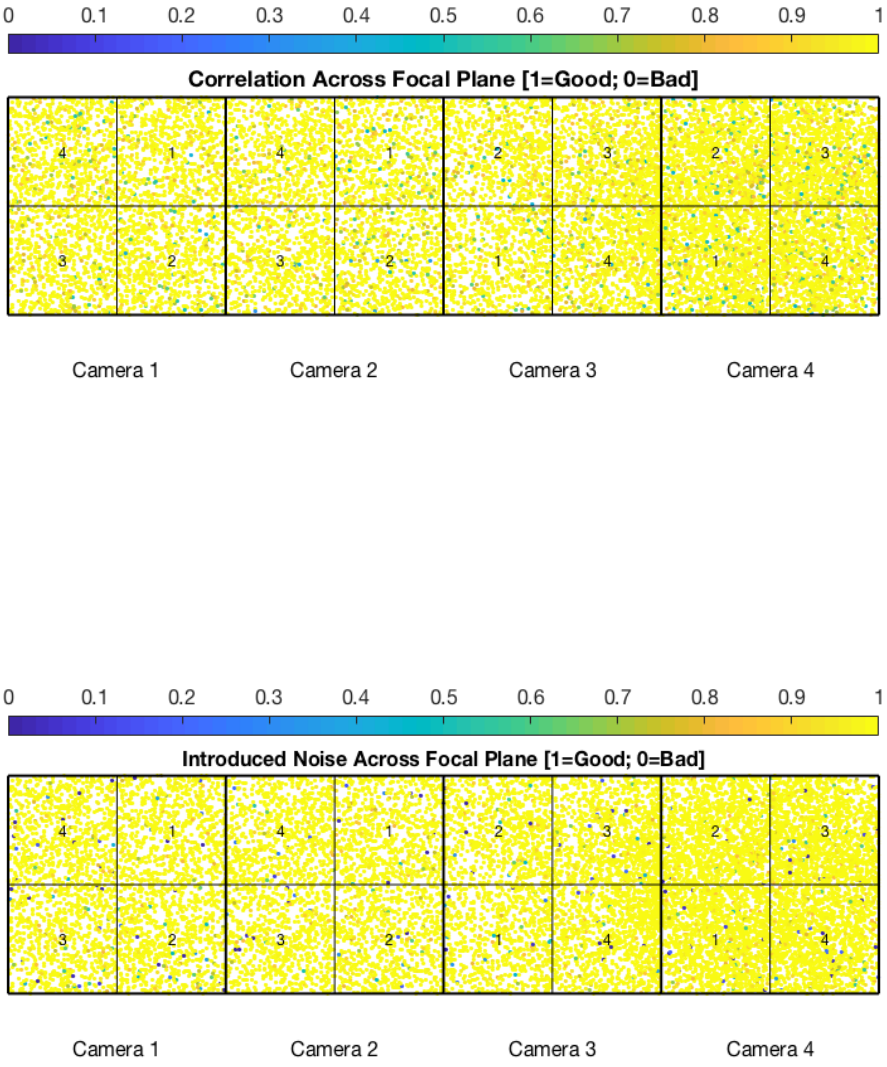

Figure 5: PDC residual correlation goodness metric (top panel) and PDC introduced noise goodness metric (bottom panel). The metric values are shown on a focal plane map indicating the camera and CCD location of each target. The correlation goodness metric is calibrated such that a value of 0.8 and above means there is less than 10% mean absolute correlation between the target under study and all other targets on the CCD. The introduced noise metric is calibrated such that a value of 0.8 and above implies that the power in broad-band introduced noise due to PDC is less than the level of uncertainties in the flux values.

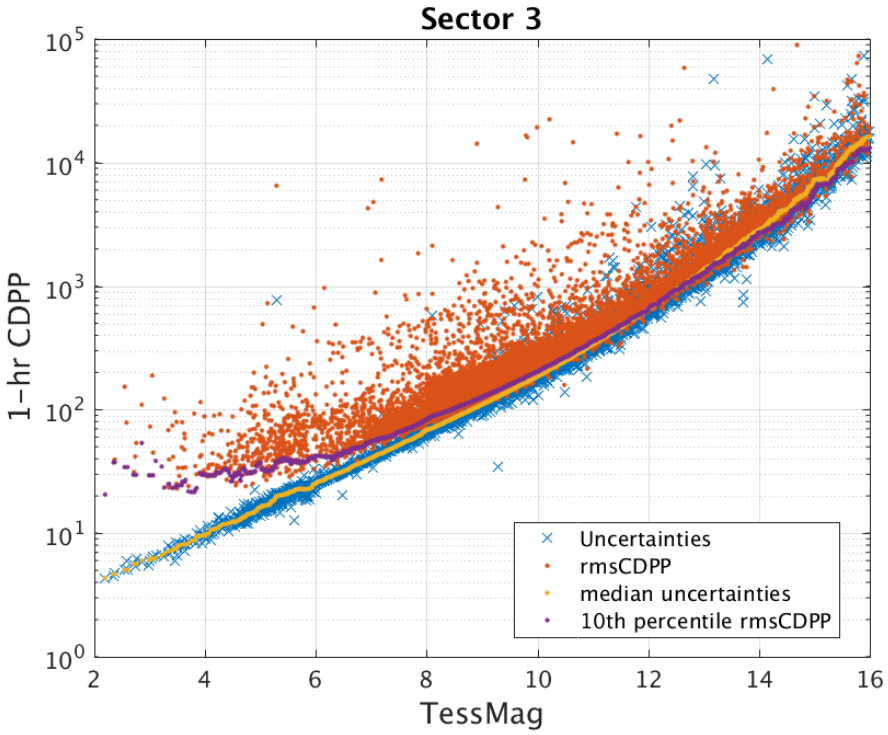

Figure 6: 1-hour CDPP. The red points are the RMS CDPP measurements for the 15,993 light curves from Sector 3 plotted as a function of TESS magnitude. The blue x's are the uncertainties, scaled to 1-hour timescale. The purple curve is a moving 10th percentile of the RMS CDPP measurements, and the gold curve is a moving median of the 1-hr uncertainties.

variations <1% after cotrending. Cadences with MAD PDC flux values greater than 1 10 ^{3} were excluded from the final run of the pipeline. See Figure 4 for comparison of the MAD PDC flux statistic before and after selecting cadences for manual excludes.

FFIs were only marked with bit 6 (Reaction Wheel Desaturation Events). Only one or two FFIs are affected by each momentum dump.

3 Anomalous Effects

3.1 Smear Correction Issues

1. Camera 2, CCD 1, Columns 279–284: There is a slight excess of charge in top of the virtual smear rows in these columns, which results in an over-correction of the smear. The source of this charge is unclear, but may be related to the bright star in the lower buffer rows at Column 284, partly visible in the science imaging region.

2. Camera 2, CCD 1, Column 459: There is excess charge in the virtual smear region centered on Column 459, Row 2062. The source of this effect is unclear, but the charge causes a slight over-correction of the smear in this and adjacent columns.

3. Camera 2, CCD 3, Column 1942: There is a bright star in the upper buffer rows, which bleeds slightly into the upper serial register and effects the smear rows in this column.

We have also observed some moderately bright stars in the upper buffer rows that affect the first row of the virtual smear region. However, the smear correction is robust against these cases and is subtracted correctly.

3.2 Black Flutter

During science observations, flutter in the mean black level was observed in Camera 1, CCD 1 and CCD 2, cadences 123900 to 129015, and Camera 4, CCD 2, cadences 121615 to 129465. The same effect was also seen in Camera 2, CCD 1 and CCD 2 during early periods of ACS testing. See the Instrument Handbook for more details about overclock flutter.

3.3 Fireflies and Fireworks

Table 2 lists all firefly and fireworks events for Sector 3. These phenomena are small, spatially extended, comet-like features in the images that may appear one or two at a time (fireflies) or in large groups (fireworks). See the Instrument Handbook for a complete description.

Table 2: Sector Fireflies and Fireworks

FFI Start	FFI End	Cameras	Description
2018265035941	2018265042941	4	single firefly
2018265125941	2018265132941	2, 3	single firefly
2018265195941	2018265202941	1	single firefly
2018272075940	2018272072940	3	single firefly
2018273095940	2018273102940	1, 2, 3, 4	fireworks
2018275175940	2018275182940	2	single firefly
2018276072940	2018276072940	2, 3	fireflies
2018280155940	2018280165940	2, 3, 4	fireflies
2018287205940	2018287212940	2	single firefly
2018289155940	2018289162940	1, 2, 3	fireflies

3.4 Timing Precision and Accuracy

The spacecraft clock slowly drifts relative to UTC time at a rate of a few 10s of milliseconds per day. The spacecraft clock kernel is used to correct this difference based on the measured drift rate. However, the clock kernel used to process Sector 3 data has a slight error in this measurement, resulting from extrapolation of timing measurements made during Sector 1. The reported TJD values in all data products are therefore offset by 1.2 seconds at the end of orbit 14 (2018-10-17 UTC). This error also implies that the durations of individual cadences are underestimated by about 20 microseconds. This issue will be corrected if the data are reprocessed in a future data release.

4 Pipeline Performance and Results

4.1 Light Curves and Photometric Precision

Figure 5 gives the PDC goodness metrics for residual correlation and introduced noise on a scale between 0 (bad) and 1 (good). The performance of PDC is very good and generally uniform over most of the field of view. As in data release 1, the goodness metrics reported in the light curve files are uncalibrated and should not be considered reliable–the calibrated goodness metrics are shown in Figure 5 and available in a supplemental file with these release notes.

Figure 6 shows the achieved Combined Differential Photometric Precision (CDPP) at 1-hour timescales for all targets. As in Sector 1, the dominant systematic uncertainty is pointing jitter.

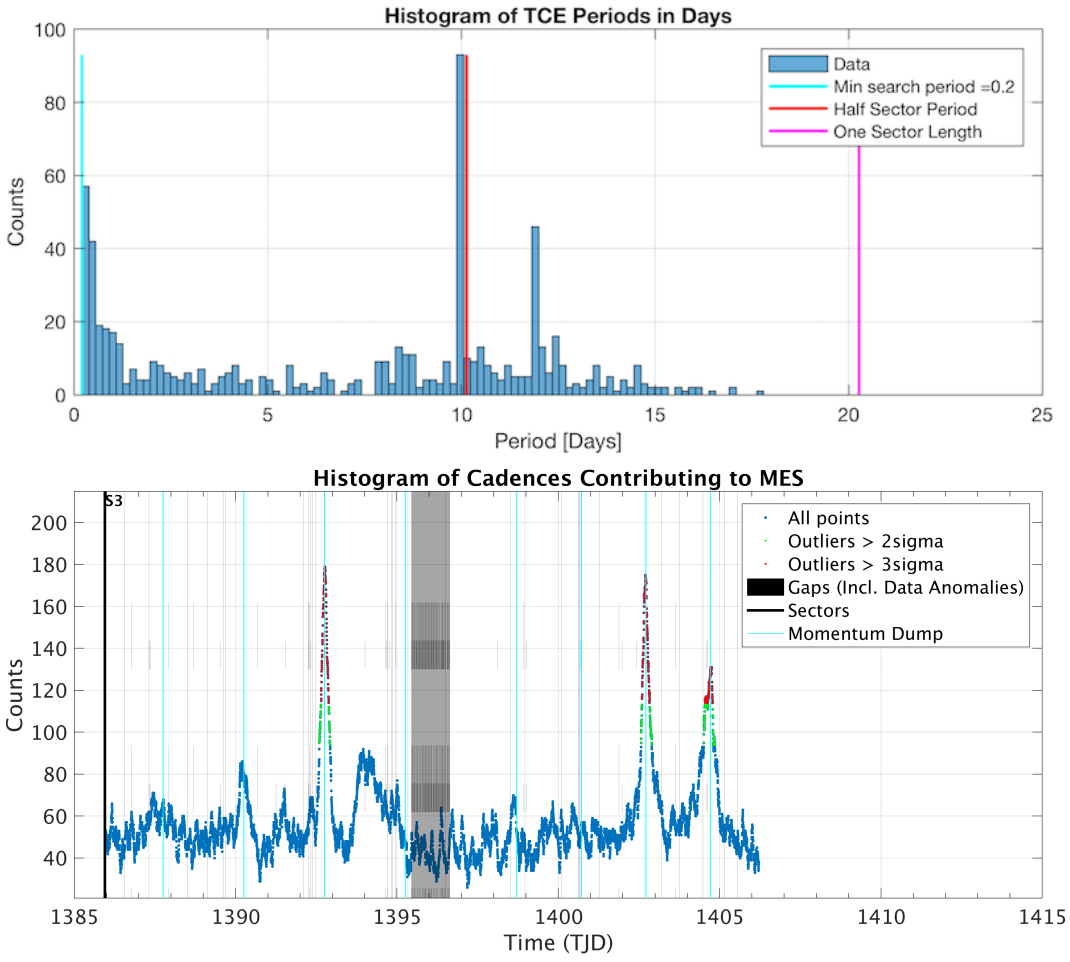

Figure 7: Top Panel: Histogram of orbital periods for 704 TCEs identified in TPS in Sector 3. Bottom Panel: Number of TCEs at a given cadence exhibiting a transit signal. Isolated peaks are associated with single events that result in numerous spurious TCEs. Here, the peaks align with momentum dumps that are spaced at integer multiples of 2.5 days. This accounts for the narrow spikes in the orbital period histogram at 10 and 12 days.

4.2 Transit Search and Data Validation

In Sector 3, the light curves of 15,993 targets were subjected to the transit search in TPS. Of these, Threshold Crossing Events (TCEs) at the 7.1σ level were generated for 704 targets.

The top panel of Figure 7 shows the distribution of orbital periods for the TPS TCEs found in Sector 3. Narrow peaks in the histogram occur at approximately 10 and 12 days. These periods are associated with momentum dumps in each of the two orbits, and are mainly caused by pointing excursions and gaps in the light curves. This is confirmed by the bottom panel of Figure 7, which shows the number of TCEs at a given cadence that exhibit a transit signal—the isolated peaks are close to the times of momentum dumps.

A search for additional TCEs in potential multiple planet systems was conducted in DV through calls to TPS. A total of 1025 TCEs were ultimately identified in the SPOC pipeline on 704 unique target stars. Table 3 provides a breakdown of the number of TCEs by target. Note that targets with large numbers of TCEs are likely to include false positives.

Table 3: Sector 3 TCE Numbers

Number of TCEs	Number of Targets	Total TCEs
1	451	451
2	196	392
3	47	141
4	9	36
5	1	5
–	704	1025

Figure 8 shows the distribution of transit depths derived from limb-darkened transiting planet model fits for TCEs with SNR $> 7.1\,\sigma$. The model transit depths range down to the order of 100 ppm, but the bulk of the transit depths are considerably larger.

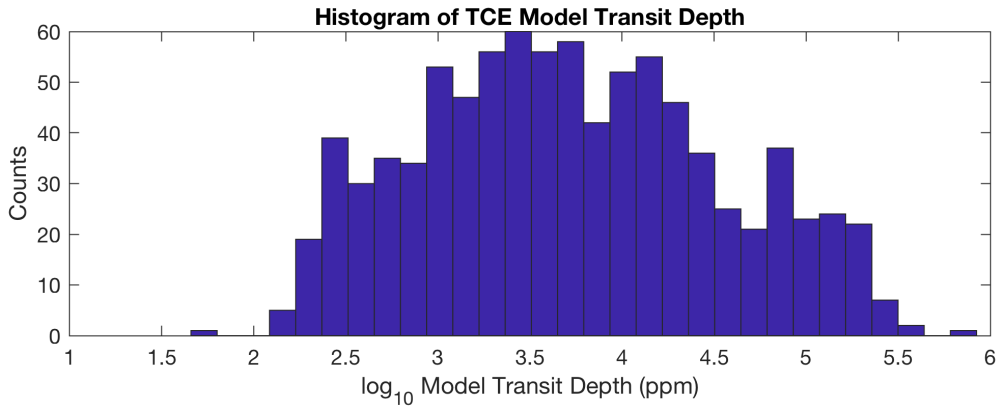

Figure 8: Histogram of limb-darkened transiting planet model transit depth for 886 TCEs with SNR $> 7.1\,\sigma$. Transit depth is displayed on a logarithmic scale in units of ppm.

References

Jenkins, J. M. 2017, Kepler Data Processing Handbook: Overview of the Science Operations Center, Tech. rep., NASA Ames Research Center

Jenkins, J. M., Twicken, J. D., McCauliff, S., et al. 2016, in Proc. SPIE, Vol. 9913, Software and Cyberinfrastructure for Astronomy IV, 99133E

Li, J., Tenenbaum, P., Twicken, J. D., et al. 2019, *PASP*, 131, 024506

Twicken, J. D., Catanzarite, J. H., Clarke, B. D., et al. 2018, *PASP*, 130, 064502

Vanderspek, R., Doty, J., Fausnaugh, M., & Villaseñor, J. 2018, TESS Instrument Handbook, Tech. rep., Kavli Institute for Astrophysics and Space Science, Massachusetts Institute of Technology

Acronyms and Abbreviation List

BTJD Barycentric-corrected TESS Julian Date

CAL Calibration Pipeline Module

CBV Cotrending Basis Vector

CCD Charge Coupled Device

CDPP Combined Differential Photometric Precision

COA Compute Optimal Aperture Pipeline Module

CSCI Computer Software Configuration Item

CTE Charge Transfer Efficiency

Dec Declination

DR Data Release

DV Data Validation Pipeline Module

DVA Differential Velocity Aberration

FFI Full Frame Image

FIN FFI Index Number

FITS Flexible Image Transport System

FOV Field of View

FPG Focal Plane Geometry model

KDPH Kepler Data Processing Handbook

KIH Kepler Instrument Handbook

KOI Kepler Object of Interest

MAD Median Absolute Deviation

MAP Maximum A Posteriori

MAST Mikulski Archive for Space Telescopes

MES Multiple Event Statistic

NAS NASA Advanced Supercomputing Division

PA Photometric Analysis Pipeline Module

PDC Pre-Search Data Conditioning Pipeline Module

PDC-MAP Pre-Search Data Conditioning Maximum A Posteriori algorithm

PDC-msMAP Pre-Search Data Conditioning Multiscale Maximum A Posteriori algorithm

PDF Portable Document Format

POC Payload Operations Center

POU Propagation of Uncertainties

ppm Parts-per-million

PRF Pixel Response Function

RA Right Ascension

RMS Root Mean Square

SAP Simple Aperture Photometry

SDPDD Science Data Product Description Document

SNR Signal-to-Noise Ratio

SPOC Science Processing Operations Center

SVD Singular Value Decomposition

TCE Threshold Crossing Event

TESS Transiting Exoplanet Survey Satellite

TIC TESS Input Catalog

TIH TESS Instrument Handbook

TJD TESS Julian Date

TOI TESS Object of Interest

TPS Transiting Planet Search Pipeline Module

UTC Coordinated Universal Time

XML Extensible Markup Language